HHS Public Access

Author manuscript

Cell Rep. Author manuscript; available in PMC 2021 February 17.

Published in final edited form as:

Cell Rep. 2021 January 26; 34(4): 108682. doi:10.1016/j.celrep.2020.108682.

Polyclonal epitope mapping reveals temporal dynamics and diversity of human antibody responses to H5N1 vaccination

Julianna Han[1], **Aaron J. Schmitz**[2], **Sara T. Richey**[1], **Ya-Nan Dai**[2], **Hannah L. Turner**[1], **Bassem M. Mohammed**[2], **Daved H. Fremont**[2,3,4], **Ali H. Ellebedy**[2,4], **Andrew B. Ward**[1,5,*]

[1]Department of Integrative Structural and Computational Biology, The Scripps Research Institute, La Jolla, CA 92037, USA

[2]Department of Pathology and Immunology, Washington University School of Medicine, St. Louis, MO 63110, USA

[3]Department of Biochemistry & Molecular Biophysics, Washington University School of Medicine, St. Louis, MO 63110, USA

[4]Department of Molecular Microbiology, Washington University School of Medicine, St. Louis, MO 63110, USA

[5]Lead contact

SUMMARY

Novel influenza A virus (IAV) strains elicit recall immune responses to conserved epitopes, making them favorable antigenic choices for universal influenza virus vaccines. Evaluating these immunogens requires a thorough understanding of the antigenic sites targeted by the polyclonal antibody (pAb) response, which single-particle electron microscopy (EM) can sensitively detect. In this study, we employ EM polyclonal epitope mapping (EMPEM) to extensively characterize the pAb response to hemagglutinin (HA) after H5N1 immunization in humans. Cross-reactive pAbs originating from memory B cells immediately bound the stem of HA and persisted for more than a year after vaccination. In contrast, *de novo* pAb responses to multiple sites on the head of HA, targeting previously determined key neutralizing sites on H5 HA, expanded after the second immunization and waned quickly. Thus, EMPEM provides a robust tool for comprehensively tracking the specificity and durability of immune responses elicited by novel universal influenza vaccine candidates.

*Correspondence: andrew@scripps.edu.

AUTHOR CONTRIBUTIONS

J.H., A.B.W., and A.H.E. conceptualized the project. J.H. designed and performed EMPEM experiments, microscopy, and data processing. A.H.E. performed serological studies and advised on the project. A.J.S. produced mAbs. Y.-N.D. performed bio-layer interferometry and surface plasmon resonance experiments and analyzed data. S.T.R., H.L.T., and B.M.M. assisted with EMPEM experiments and microscopy. D.H.F. advised on the project. A.B.W. supervised the project. J.H. wrote the manuscript, A.B.W. edited the manuscript, and all authors provided feedback for the manuscript.

DECLARATION OF INTERESTS

A.H.E. is a consultant for InBios and Fimbrion Therapeutics. The Ellebedy laboratory received funding under sponsored research agreements from Emergent BioSolutions. The remaining authors declare no competing interests.

SUPPLEMENTAL INFORMATION

Supplemental Information can be found online at https://doi.org/10.1016/j.celrep.2020.108682.

In Brief

Vaccines containing novel influenza strains such as H5N1 are promising candidates for boosting broadly cross-reactive antibody responses in humans. Han et al. structurally characterize immunity after H5N1 vaccination in a human cohort over time, identifying polyclonal antibodies that target neutralizing sites on H5N1 or cross-react with other influenza viruses.

Graphical Abstract

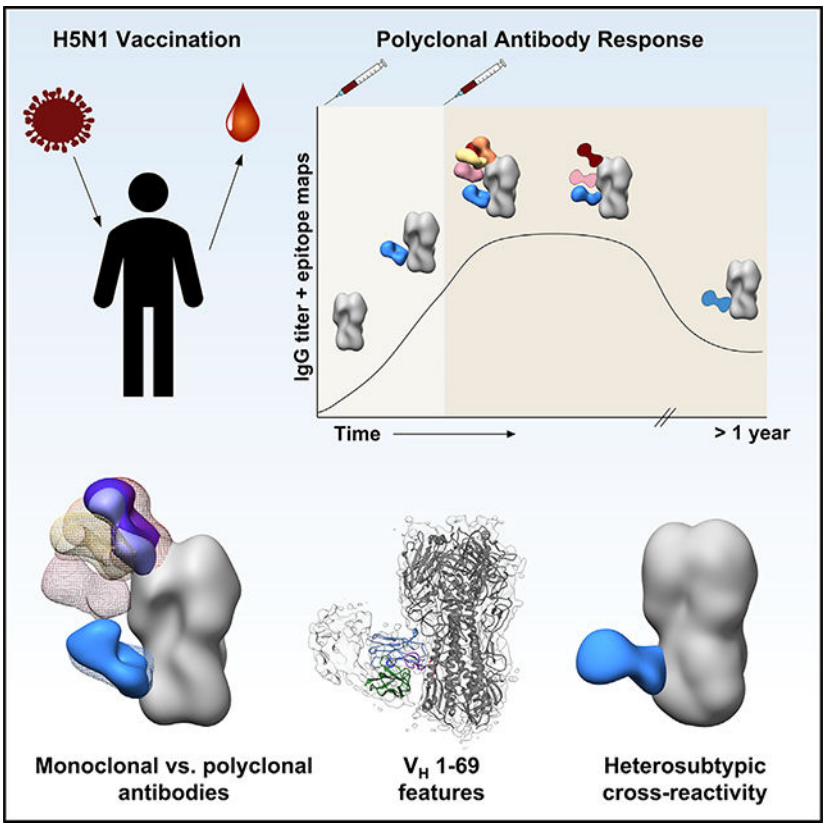

INTRODUCTION

Despite decades of endeavors to produce a lasting therapeutic and effective vaccine, seasonal influenza virus still causes a tremendous burden to public health each year, and pandemic influenza virus is a constantly looming threat. To understand the range of protection needed for seasonal and universal influenza virus vaccines (vaccines that can generate protection against a broad array of influenza virus strains), we need a thorough characterization of humoral immune responses to influenza virus vaccination (Erbelding et al., 2018).

Because of antigenic drift, that is, the ability of influenza virus to mutate in response to selection pressures imposed by host immune systems, seasonal influenza virus vaccines must be reformulated yearly and still result in only 10%–60% efficacy (Centers for Disease Control and Prevention, 2020). Current vaccines are strain-specific, eliciting antibody responses primarily to the variable head region of hemagglutinin (HA). This creates a

challenge for generating vaccines to potentially pandemic strains, since it is almost impossible to predict which strain can cause a pandemic.

Highly pathogenic avian influenza (HPAI) H5N1 viruses have been periodically crossing the species barrier from birds into humans, causing serious lower respiratory tract infections and viral pneumonia (Claas et al., 1998; Peiris et al., 2007; Cowling et al., 2013). H5N1 infections in humans result in up to 50%–60% mortality among clinically confirmed cases, in large part due to little pre-existing immunity to avian influenza A virus (IAV) strains in the human population (World Health Organization, 2020). However, due to frequent exposure to seasonal influenza virus HAs, humans harbor memory B cells that are directed against epitopes shared between such HAs and H5 HA. These epitopes predominantly reside within the conserved stem region of HA and are the targets of broadly reactive antibodies (Throsby et al., 2008; Ekiert et al., 2009). A major strategy for universal influenza vaccine design is to re-focus immune responses to the immuno-subdominant but conserved stem by immunizing with HA from non-circulating influenza virus strains, such as H5N1, thereby recalling matured memory B cells to sites shared between influenza virus subtypes (Ellebedy et al., 2014; Nachbagauer et al., 2014; Nachbagauer and Palese, 2020). Rational vaccine design of subunit-based vaccines is well suited to this endeavor, as this approach uses structural insight of epitope-paratope interactions to produce a vaccine that induces specific and focused immune responses (Burton, 2010; Impagliazzo et al., 2015; Yassine et al., 2015; Kanekiyo et al., 2019). To inform rational vaccine design, there must first be a comprehensive structural description of these conserved epitopes in complex with antibodies, as well as an understanding of the dynamics of the polyclonal antibody (pAb) response to these epitopes.

Recent advances in evaluating antibody responses have produced a clearer picture of humoral immunity to IAV, yet such techniques are still labor-intensive, time-consuming, and unable to discern the full complexity of the pAb response (Wilson and Andrews, 2012). For example, enzyme-linked immunosorbent assays (ELISAs) reveal antibody reactivity to immunogens but do not include information on targeted epitopes. Additionally, isolation and characterization of monoclonal Abs (mAbs) represent a lengthy process involving multiple techniques and, due to limited sampling ability, typically only represents a subset of the pAb response. The application of single-particle electron microscopy (EM) to structurally characterize heterogeneous pAb immune complexes from low to high resolution yields unprecedented insight into polyclonal immune responses following IAV vaccination. We previously designed and implemented EM polyclonal epitope mapping (EMPEM) to discern the polyclonal immune response of rabbits and non-human primates to vaccination with HIV immunogens (Bianchi et al., 2018; Cirelli et al., 2019; Moyer et al., 2020; Nogal et al., 2020). This structure-based strategy is highly efficient: sample preparation is straightforward, and the pipeline from sample collection to structural results is streamlined and expeditious, making longitudinal assessment of polyclonal responses in multiple subjects over a vaccination trial feasible.

In a previous study that characterized B cell responses of H5N1 (A/Indonesia/5/2005) vaccinated subjects, Ellebedy et al. (2020) demonstrated robust HA-specific plasmablast responses in trial participants following H5N1 vaccination with AS03 adjuvant. In these

subjects, the first dose of H5N1 vaccination elicited cross-reactive, stem-specific memory B cells and highly mutated antibodies with some microneutralization activity while the second dose elicited head-specific, naive B cells and minimally mutated antibodies with receptor binding site (RBS) neutralization activity (Ellebedy et al., 2020). In the present study, we dive deeper into the same patients and use EMPEM to map the landscape of human pAbs to HA at several time points after two doses of H5N1 vaccination from day 0 through 500. We detect persistent pAb responses to conserved epitopes on the stem domain of HA as well as pAb responses to the vulnerable sites on the head domain of HA that are also targeted during natural H5N1 infection in humans (Zuo et al., 2015). By charting the diverse and complex pAb responses to H5N1 vaccination through 500 days our study provides epitope-level insight to inform immune-focusing, rational vaccine design strategies.

RESULTS

Robust serum response to H5N1 vaccination

To assess the humoral response to vaccination with a novel strain of influenza, we obtained serum from human subjects who participated in a pandemic H5N1 vaccination trial (ClinicalTrials.gov: NCT01910519, A/Indonesia/5/2005 H5N1) (Ellebedy et al., 2020). The monovalent vaccine with Adjuvant System 03 (AS03), a squalene-in-water emulsion adjuvant, was administered in two immunizations at day 0 and day 21 (Figure 1A). Sera were collected at days 0, 7, 21, 28, 42, 100, and 500 to measure the humoral response to H5N1 vaccination (Figure 1A).

In our previous work, through analysis of isolated mAbs we distinguished naive and memory B cell dynamics of subjects 4, 28, 36, and 43 (Ellebedy et al., 2020). In the present study, we structurally characterized serum from these four subjects, with serological analyses to contextualize structural assessments. We observed an increase in H5-HA-specific serum immunoglobulin G (IgG) titers throughout the trial, with peak levels around 42 days after the first vaccination (Figures 1B and S1A). HAI titers, a measurement of the ability of HA to crosslink red blood cells through binding its receptor, sialic acid, increased after the second immunization in the four donors, suggesting that serum IgG at later time points can neutralize by blocking HA receptor binding activity (Figure 1C).

To dissect head- and stem-targeting pAbs in serum, we performed ELISAs using probes of the trimeric HA head domain alone and a chimeric construct containing H5 stem and H9 head, as described previously (Ellebedy et al., 2020). Immediately following the first immunization, stem-specific serum IgG levels increased and remained high through 100 days after vaccination (Figure 1D). Conversely, head-specific serum IgG levels remained around baseline after the first immunization but rose drastically after the second immunization and remained elevated through 100 days after vaccination (Figure 1D). Monoclonal antibodies isolated from plasmablasts at days 7 and 28 from subjects 4, 28, 36, and 43 supported the head- and stem-specific dichotomy: day 7 mAbs targeted the stem while day 28 mAbs targeted the head of HA (Ellebedy et al., 2020). Affinity-matured B cells produce antibodies with high somatic hypermutation (SHM) and strong affinity, while naive or new memory B cells produce antibodies with minimal mutations and low affinity (Kurosaki et al., 2015). We observed that day 7 mAbs had higher SHM loads (determined

previously: Ellebedy et al., 2020), stronger affinities, and slower off-rates than did day 28 mAbs (Figures S1B–S1E). These data suggest that affinity-matured memory B cells targeting the stem of HA responded quickly to novel H5N1 antigen but naive or minimally mutated memory B cells responded to the head of HA only after a second exposure to H5N1 antigen (Ellebedy et al., 2020).

While traditional serological analyses generate useful information about binding and functionality of pAb responses as a whole, they do not reveal details about epitopes and binding specificities of individual pAbs. Thus, we used EMPEM to chart the epitope landscape targeted by pAbs over time.

pAbs elicited by H5N1 vaccination bind the stem, head, and vestigial esterase domains of HA

EMPEM is a visual proteomics method that encompasses vaccination sample collection, antibody isolation and immune complex purification, and single-particle EM image analysis (Figure 2). Following vaccination and antibody purification, we complexed HA with a large molar excess of Fab and purified immune complexes by size exclusion chromatography, where a protein peak corresponding to the immune complex and unbound trimer separated from the excess Fab peak (Figures 2A and S2). During EM imaging and data processing, we collected micrographs, extracted single particles, and categorized particles by similarity through multiple rounds of 2D classification (Figure 2B). In the 2D class averages, we can already detect numerous pAb specificities and assign targeted epitopes. Next, we performed multiple iterations of 3D classification and refinement of immune complexes. Finally, we represented 3D reconstructions of each pAb specificity on one protomer of the HA trimer to generate epitope landscapes of each subject and time point (Figure 2B).

To characterize the dynamics of the pAb response to H5N1 vaccination, we performed EMPEM on serum samples from four subjects. For the first subject (subject 4), we processed sera from days 0, 7, 21, 28, 42, and 500 and complexed pAbs with the vaccine strain-matched HA (A/Indonesia/5/2005, Figures 3 and S3). At day 0, we did not observe any HA-specific pAbs in 2D class averages (Figure 3A). By day 7 and day 21, we observed stem-specific pAbs binding H5 HA (Figures 3B and 3C). These stem-specific pAbs are likely cross-reactive recalled antibodies elicited to conserved epitopes in the HA stem domain by prior seasonal influenza infection or vaccination, as day 7 mAbs were affinity matured and exhibited high SHM (Figure S1; Ellebedy et al., 2020). By day 28, 1 week after the second immunization, we observed pAbs still targeting the stem domain of HA as well as pAbs targeting the head domain at multiple angles and orientations around the RBS, lateral patch, and vestigial esterase domain (Figure 3D). By day 42, pAb responses to the RBS, vestigial esterase domain, and stem domain persisted while other head-targeting pAbs waned (Figure 3E). Finally, after day 500, stem-specific pAbs remained circulating in low abundance (Figure 3F). Overall, subject 4 recalled cross-reactive stem-specific pAbs immediately following H5N1 vaccination that persisted more than 1 year after vaccination and also elicited a transient wave of pAbs targeting the head and vestigial esterase domains after the second immunization.

We extended EMPEM analyses to three more subjects in the H5N1 vaccination trial (Figures 4 and S4). At day 0, two of the subjects (36 and 43) already showed a stem-specific pAb response to H5 HA. These pAbs must therefore have been circulating in serum before H5N1 vaccination and cross-reacted with the vaccine antigen. By day 7, all subjects recalled a strong stem-specific memory pAb response to H5 HA (Figure 4A). These are likely broadly cross-reactive pAbs elicited by previous seasonal vaccination or infection. At day 21, the day of the second immunization, subject 43 had already elicited a pAb response to the RBS of H5 HA (Figure 4A). By day 28, all subjects maintained stem-specific pAb responses (Figure 4A) while eliciting head-specific pAb responses to varying degrees. Subjects 4 and 43 exhibited pAb responses to the RBS, lateral patch, and vestigial esterase domain. Subjects 28 and 36 had a less diverse head-specific response to the RBS or to the mid-lateral region of the head. At intermediate time points (day 42 for subject 4 and day 100 for subject 43; serum was unavailable for subjects 28 and 36 at these time points), pAbs targeting the RBS, vestigial esterase, and stem domains remained in circulation (Figure 4A). Expansion of pAbs against epitopes on the head of HA was consistent with the increase in HAI titers after the second immunization (Figures 1C and 4). After 500 days all subjects with serum available demonstrated a lasting stem-specific pAb response (Figure 4), and subject 28 also displayed an RBS-specific pAb response.

In summary, the landscape of pAbs responding to H5N1 vaccination followed two concurrent trends: stem-specific pAbs targeted H5 HA from baseline through 500 days (Figure 4B). These pAbs may have been circulating in serum before vaccination, recalled shortly after the first immunization, or newly elicited after the second immunization. Head-specific pAbs expanded after the second immunization, targeting the RBS, lateral patch, mid-lateral head region, and vestigial esterase region, and they waned quickly as the trial progressed, with the pAbs targeting more conserved regions enduring longer (Figure 4B). Taken together, these data demonstrate that H5N1 vaccination elicits a prominent and prolonged pAb response to the conserved stem domain of HA, as well as a more diverse and transient pAb response to the variable, immunodominant head domain of HA.

The kinetics of the polyclonal response mapped by EM are consistent with serum ELISA and HAI data showing that stem-specific antibodies were already present at day 0 and continually increased during the course of vaccination, while head-specific antibodies and HAI^{+} antibodies were substantially present only after the second immunization (Figures 1C, 1D, and 4). By day 42 or 100, serum IgG binding titers were still high for the majority of subjects but were declining for donors 4 and 43 (Figures 1B and 1D). In agreement, the EM-mapped pAb landscape at these intermediate time points was less diverse for donors 4 and 43. Perhaps more dominant pAbs persist at high levels through these time points while the more transient pAbs wane.

H5N1 vaccine-elicited mAbs target discrete regions on HA and share footprints with pAbs

Previously, Ellebedy et al. (2020) characterized a panel of mAbs isolated from these subjects and identified a biphasic response: day 7 mAbs exclusively targeted the stem of HA with high SHM and breadth, while day 28 mAbs targeted the head of HA with little SHM and strain- or subtype-specific reactivity. In this study, we complexed mAbs at days 7 and 28

from subjects 4 and 43 with H5 HA (A/Indonesia/5/2005) to compare the binding footprints and orientations with pAbs at day 28. All day 7 mAbs used the heavy chain variable region V_H1–69 germline and targeted the same footprint on the stem of HA (Figures 5A, S5A, and S5B). While day 28 mAbs utilized a mixture of germlines, including three mAbs with V_H3–33, six of the seven mAbs targeted the same footprint on the RBS of HA (Figures 5C, S5A, and S5C). The seventh mAb targeted the vestigial esterase domain of HA (Figure 5B). Upon comparing the footprints of these mAbs with day 28 pAbs from subjects 4 and 43, we observed that each day 7 mAbs overlapped almost perfectly with the blue stem-specific pAbs (Figure 5D). Additionally, each day 28 RBS-specific mAbs overlapped almost exclusively with each other and were represented by pAbs (Figure 5D). Finally, while we were unable to obtain a 3D reconstruction of day 28 1B02 mAbs, 2D class averages confirmed that they bound the vestigial esterase domain in the same vicinity as the vestigial esterase-specific pAbs (Figures 5B and 5D).

To compare the cross-reactive potential of mAbs from days 7 and 28, we complexed each mAb with HAs from heterosubtypic strains, including H1N1 (A/California/04/2009), H2N2 (A/Singapore/1/1957), and H3N2 (A/Singapore/INFIMH-16–0019/2016; Figure 5E). As expected, day 7 stem-specific mAbs demonstrated broad cross-reactivity, binding H5, H1, and H2 HAs, while day 28 head-specific mAbs demonstrated subtype- or strain-specific reactivity, binding only H5 HA.

Out of six pAb footprints identified by EMPEM only three were represented by mAbs, suggesting that mAb analysis did not fully recapitulate the diversity of the polyclonal response. Additionally, while day 28 mAbs targeted the head of HA almost exclusively (Figures 5C and 5D), ELISA data of serum IgG also demonstrated binding activity to the stem of HA at day 28 (Figure 1D), further highlighting the role of pAb mapping to elucidate the complete polyclonal response at the serum level. However, mAb data provide valuable functional information and are complementary with EMPEM data; taken together, these results suggest that pAbs at day 7 are dominated by robust and broadly cross-reactive V_H1–69 stem responses while pAbs at day 28 target variable head epitopes and continue to target broadly cross-reactive stem epitopes.

Cross-reactive immunity by H5N1 vaccine-elicited pAbs

After characterizing polyclonal epitope landscapes at low resolution, we next aimed to decipher molecular details of epitope-paratope interactions through cryoEMPEM on polyclonal sera. As serum samples were already depleted from our previous study as well as negative stain EMPEM, we only had enough serum to perform this analysis on pAbs from subject 4 at day 28. We processed cryoEM data using a focused classification data analysis pipeline (Figure S6A) (Zivanov et al., 2018) that enabled detection and reconstruction of minority immune complexes from total particles.

We discerned high-resolution immune complexes of pAbs from subject 4 at day 28 that targeted the stem and multiple sites on the head of HA from a single cryoEM sample (Figures 6A, 6B, and S6B–S6E). Importantly, these epitopes corroborated the negative stain epitope landscape for subject 4 at day 28, demonstrating that the lower resolution negative stain methodology was sufficient to observe all epitopes. Due to limited serum sample

availability each immune complex in our cryoEM images was present in low abundance—the stem specificity accounted for ~4% while each of the three head specificities represented just ~1%–2% of the total particles. Nevertheless, focused classification enabled us to detect and reconstruct these antibodyepitope interactions. The RBS-binding pAb plugged the receptor binding pocket on HA, likely blocking receptor binding (red epitope, Figures 6A, 6B, and S6B). The remaining head-binding pAbs targeted the lateral patch (yellow) and vestigial esterase (pink) epitopes (Figures 6A, 6B, and S6B).

Intriguingly, the stem-specific pAb (Figures 6A–6C) bound in almost the exact same location and orientation as CR9114, a V_H1–69 prototypical stem-directed broadly neutralizing Ab (Figure S6F) (Dreyfus et al., 2012; Lee and Wilson, 2015). The V_H1–69 lineage broadly reactive mAb 1C01 from subject 4 superimposed almost perfectly with the stem-binding pAb, suggesting that this mAb is part of the polyclonal response at that specificity (Figures 5A and S6G). Upon docking the predicted structure of the variable regions of 1C01 mAb into the cryoEM pAb density, we observed that the pAb interaction appears to be mediated by the signature IFY motif in CDR H2 and H3 that likely interacts with H18 in HA1 and W21 in HA2 (Figures 6C–6D) (Dreyfus et al., 2012; Lee and Wilson, 2015). Thus, high-resolution cryoEM mapping identified a broadly neutralizing CR9114-like stem response in polyclonal sera following H5N1 vaccination, supporting components of the novel H5 antigen as a prime candidate for a universal influenza vaccine.

The major vulnerable sites (VSs) on the head of H5 HA have been determined previously based on protective neutralizing mAbs isolated from humans who recovered from HPAI H5N1 infections (VS1–VS3) and mice immunized with HPAI H5N1 (VS4) (Zhu et al., 2013; Zuo et al., 2015). We mapped these vulnerable sites onto the H5 HA trimer and compared them to negative stain EMPEM epitopes (Figure 7A). The footprints of H5N1 vaccine-elicited pAbs determined by both negative stain and cryoEM encompassed each of the vulnerable sites, including the RBS in VS2 (red), lateral patch in VS1 (yellow), and vestigial esterase domain bridging VS3 and VS4 (pink; Figures 6A, 6B, and 7A). The major vulnerable sites were determined based on protective neutralization activity. Although antibody responses to the stem can have neutralizing activity, they can also protect through effector functions such as antibody-dependent cell-mediated cytotoxicity and antibody-dependent cellular phagocytosis (DiLillo et al., 2014; Cox et al., 2016; Coughlan and Palese, 2018; Boudreau and Alter, 2019). H5N1 vaccine-elicited pAbs also targeted the stem domain, but they were not represented in the characterization of neutralizing responses to H5N1 infection (Zuo et al., 2015). In summary, H5N1 vaccine-elicited head pAb responses mimic homosubtypic broadly neutralizing mAb responses to natural HPAI H5N1 infection.

To investigate the heterosubtypic breadth of polyclonal antibodies elicited by H5N1 vaccination, we examined the ability of pAbs from donor 43 at day 21 to bind H1 HA using EMPEM (Figures 7B and S7). We assessed cross-reactivity to the antigenically drifted A/Michigan/45/2015 (H1N1) HA that emerged in 2015. As serum samples were isolated from subjects in 2013, the subjects were naive to this H1N1 strain. Due to limited serum sample availability, we were only able to perform this analysis on one time point. However, we saw pAbs targeting the broadly cross-reactive V_H1–69 epitope on the stem of H1 HA, suggesting that H5N1 vaccination elicits pAbs that recognize multiple influenza virus subtypes.

Moreover, these results demonstrate that EMPEM can sensitively detect pAb responses to strains of different subtypes than the vaccine strain.

To compare the epitope landscapes after H5N1 vaccination with known broadly neutralizing responses, we superimposed H5N1-reactive broadly neutralizing antibodies (bnAbs) with pAbs from subject 4 at day 28 (Figure 7C) (Sun et al., 2014; Lee and Wilson, 2015). As described above, the bnAb CR9114 that protects against both influenza A and B viruses mapped almost exactly with vaccine-elicited stem pAbs and V_H1–69 mAbs (Figures S6F, S6G, and 7C) (Dreyfus et al., 2012). Similarly, bnAbs toward the vestigial esterase (H5M9, pan-H5N1 reactive) and RBS (S139/1, group 1 and 2 cross-reactivity against H1, H2, H3, H5, H9, and H13) also overlapped footprints and angles of approach with pAbs (Figure 7C) (Yoshida et al., 2009; Lee et al., 2012; Zhu et al., 2013). These results suggest that H5N1 vaccination elicits pAb responses to regions of broadly neutralizing epitopes.

DISCUSSION

Comprehensive mapping of the HA epitopes targeted by the pAb response remains a major gap in our understanding of the human B cell response to influenza viruses. EMPEM is a unique modality that sensitively detects minority antigen-specific antibodies, providing a comprehensive landscape of the polyclonal immune response. In this study, we show that EMPEM can directly inform rational design of a universal influenza vaccine by extensive characterization of pAb responses to a vaccine derived from non-circulating IAV strains, such as H5N1. While we have performed EMPEM on rabbit and NHP sera, herein we report the first study using our structure-based method to comprehensively map the polyclonal response to an avian influenza virus vaccine in humans (Bianchi et al., 2018; Cirelli et al., 2019; Moyer et al., 2020; Nogal et al., 2020).

Complementary serological techniques inform our understanding of the pAb response to influenza virus vaccination, and EMPEM contextualizes data from these traditional methods. In this study, ELISA binding titers indicated a strong stem-specific response that increased during the course of H5N1 vaccination but a low initial head-specific response that expanded after the second immunization (Figure 1D). HAI^+ antibodies were only detected after the second immunization (Figure 1C). Ellebedy et al. (2020) also determined that mAbs at day 7 had higher levels of SHM and were likely generated by highly mutated memory B cells, while mAbs at day 28 were strain-specific and were produced from naive or recently generated memory B cells.

EMPEM analyses corroborated and extended these observations by describing specific epitopes targeted on the head and stem domains of HA, including five unique epitopes targeted across the head domain that incorporate every known vulnerable site on H5 HA (Figure 7A). Our analyses also elucidated atomic level detail of the IFY motif in persistent, broadly neutralizing stem pAbs with V_H1–69 CR9114-like qualities, differentiated overlapping antibodies and angles of approach to similar epitopes, and monitored the kinetics of each response during the course of vaccination (Figures 3 and 4). Additionally, the number of unique specificities in the pAb response began declining by day 42 or 100 in two donors, supported by ELISA data also showing declining serum IgG titers for these

donors. These results demonstrate that EMPEM can track the kinetics of individual pAb specificities.

Current universal influenza vaccines focus on eliciting bnAbs against the conserved stem of HA. However, influenza viruses can escape from stem-targeting antibodies, although this may be less likely for group 1 HA strains (Wu et al., 2020; Anderson et al., 2017). Conserved regions on the head of HA, such as the RBS, can also play an important role in universal protection (Krammer, 2019). Therefore, eliciting bnAbs to both conserved head and stem epitopes could strengthen universal protection and limit the development of resistance to single epitopes. Interestingly, after the first H5N1 immunization, subject 43 elicited an RBS-directed pAb circulating by day 21 (Figure 4). As this was subject 43's first exposure to novel H5 HA, it is possible that the immunization elicited cross-reactive memory B cell responses to conserved sites on the HA head. Additionally, subject 28 still had low levels of pAbs targeting the RBS region circulating 1 year after vaccination (Figure 4). As these pAbs may recognize conserved aspects of the RBS, they may have been derived from a new memory B cell population that matured and differentiated into long-lived plasma cells. In the future, we can test this hypothesis by tracking the evolution of RBS-specific mAbs from subject 28 during the course of the trial.

By matching binding specificities of mAbs and pAbs from corresponding serum samples, we can evaluate how well mAbs represent the pAb response and extrapolate functional properties of pAbs. mAbs are usually isolated from plasmablasts or memory B cells and thus may not encompass the diversity of antibodies present in serum. In this study, mAb analyses demonstrated a biphasic response to H5N1 vaccination; mAbs isolated at day 7 exclusively bound the stem domain while mAbs from day 28 specifically bound the head domain of HA. Interestingly, the biphasic response to HA was not fully recapitulated by EMPEM data; subject 43 also targeted the head after the first immunization, and a large proportion of pAbs still targeted the stem after the second immunization (Figures 3 and 4). Moreover, EM mapped day 28 mAbs bound almost exclusively to the RBS, while day 28 EMPEM results demonstrated a diverse pAb response to multiple head epitopes (Figures 4 and 5) (Ellebedy et al., 2020). We used full-length H5 HA as the probe for isolating mAbs; perhaps B cell receptor (BCRs) recognize the RBS more readily than the stem, resulting in biased isolation of head-specific B cells. Alternatively, even though the quantity of stem pAbs did not diminish, it is possible that the expansion of head-specific B cells at day 28 outnumbered stem-specific B cells, resulting in preferential isolation of head-specific B cells. Finally, due to clonal expansion, mAb isolation may be biased toward more dominant B cell clones, whereas EMPEM evaluates the total IgG pool and can identify minority epitopes. Nevertheless, we can extract crucial details about the polyclonal response through mAb analysis; day 7 pAbs consist of broadly reactive V_H1–69 antibodies. mAb analysis provides powerful functional details of antibodies, but EMPEM is necessary to recapitulate the complexity and dynamics of the pAb response.

Humans have lifelong exposure history with influenza viruses and elicit immune responses mostly to the immunodominant and drifting head of HA (Krammer, 2019). An individual's first influenza virus infection strongly biases their immune response to subsequent, drifted influenza virus strains, resulting in person-to-person variation (Li et al., 2013; Andrews et

al., 2015; Gostic et al., 2016, 2019). Additionally, single Ab specificities may functionally dominate the pAb response, rendering other specificities inconsequential (Li et al., 2013; Huang et al., 2015; Lee et al., 2019). This phenomenon also differs between individuals and may be influenced by pre-exposure history. Our study establishes EMPEM as a powerful new tool for gauging pre-existing immunity and variation between individuals by mapping bulk influenza-directed pAb responses at baseline and during the course of vaccination to multiple antigens as well as distinguishing differences in epitope targets per individual. Our EMPEM results identified pre-existing, cross-reactive stem pAbs at baseline in half of the subjects, elicitation and persistence of cross-reactive stem pAbs in all subjects after primary exposure, and expansion of a decorated head response that varied in each subject after secondary exposure to H5 HA (Figures 3 and 4). In future studies with known patient ages and immune histories, EMPEM will be advantageous for dissecting pAb targets between individuals, connecting pAb differences with pre-exposure immune profiles.

As humans are immunologically naive to avian influenza virus strains, such as H5N1, primary exposure to their antigens may direct the immune response to conserved epitopes predominantly located on the stem region of HA, potentially providing broad protection against circulating and pandemic influenza virus strains (Nachbagauer and Palese, 2020). Previous studies suggested that H5N1 vaccines are poorly immunogenic and result in lower seroconversion rates compared to seasonal influenza virus vaccination, but these conclusions are mostly based off of HAI titers (Bresson et al., 2006; Treanor et al., 2006; Belshe et al., 2014). In this study, we show that low-dose inactivated H5N1 vaccination adjuvanted with AS03 elicits a potent response to highly conserved epitopes in the stem domain immediately after the first immunization that is sustained over a year after vaccination. Additionally, after the second immunization we observed a head response that targets all major neutralizing sites on the head of H5 HA, potentially enhancing protection against H5N1 strains (Figure 7A) (Zuo et al., 2015). Finally, H5N1-elicited pAbs encompass broadly neutralizing sites in the stem, esterase, and RBS of HA, emphasizing H5 HA’s utility as an antigenic candidate (Figure 7C).

Training adaptive immunity to successfully target and neutralize multiple influenza virus strains is imperative for the success of a universal influenza vaccine. This study underscores the ability of novel influenza antigens to elicit memory responses to conserved sites on HA, while also illustrating subtype-specific responses upon re-exposure to the same strain. Therefore, immunogens in a prime/boost regimen for a universal influenza vaccine should be from a different strain, such as a novel H7 antigen, to keep pAb responses trained on conserved epitopes in the stem and RBS and away from off-target recalled epitopes. Here and in future studies, EMPEM can dissect pAb responses to influenza virus vaccinations and infections with novel and seasonal strains, enabling comparison of immune responses of humans across age groups and with varying exposure histories. This extensive characterization of immune responses to influenza virus will contribute invaluable information for developing universal influenza vaccines.

STAR★METHODS

RESOURCE AVAILABILITY

Lead contact—Further information and requests for resources and reagents should be directed to and will be fulfilled by the Lead Contact, Andrew B. Ward (andrew@scripps.edu).

Materials availability—This study did not generate new unique reagents.

Data and code availability—3D EM reconstructions have been deposited to The Electron Microscopy Data Bank (emdataresource.org). The accession numbers, also listed in the Key Resources Table, are EMDataBank: EMD-22536, EMD-22537, EMD-22538, EMD-22539, EMD-22540, EMD-22541, EMD-22542, EMD-22543, EMD-22544, EMD-22545, EMD-22546, EMD-22547, EMD-22548, EMD-22549, EMD-22550, EMD-22551, EMD-22552, EMD-22553, EMD-22554, EMD-22555, EMD-22556, EMD-22557, EMD-22558, EMD-22559, EMD22560, EMD-22561, EMD-22562, EMD-22563, EMD-22564, EMD-22565, EMD-22566, EMD-22567, EMD-22568, EMD-22569, EMD-22570, EMD-22571, EMD-22572.

EXPERIMENTAL MODEL AND SUBJECT DETAILS

The vaccination trial (ClinicalTrials.gov: NCT01910519) has been described previously and was approved by the Institutional Review Board of Emory University (Ellebedy et al., 2020). Briefly, healthy adult male and female participants between 21–45 years old were immunized with monovalent inactivated A/Indonesia/05/2005 (H5N1) influenza vaccine with AS03 adjuvant provided by GlaxoSmithKline. All participants provided informed consent. Plasma and peripheral blood mononuclear cells (PBMCs) were collected at days 0, 7, 21, 28, 42, 100, and 500 after the first immunization.

METHOD DETAILS

ELISA—We coated 96-well plates with recombinant HA (A/Indonesia/5/2005) overnight at 4°C. Following HA binding, we incubated the plates at room temperature for 1 hour with blocking buffer (0.1% Tween 20, 0.5% milk powder, 3% goat serum in phosphate-buffered saline (PBS)). Next, we incubated serial dilutions of mAbs on HA-coated plates at room temperature for 2 hours followed by three washes with 0.1% Tween 20 in PBS. We added secondary goat anti-human IgG conjugated to horse radish peroxidase at 1:3000 dilution in blocking buffer to plates and incubated at room temperature for 1 hour. Finally, we washed the plates four times with 0.1% Tween 20 in PBS, added SigmaFast o-phenylenediamine solution, and measured 490nm signal using a plate reader. To distinguish head and stem responses, we used the trimeric head domain from A/Indonesia/5/2005 and chimeric HA expressing the stem from A/Indonesia/5/2005 and the head of H9 from A/guinea fowl/Hong Kong/WF10/1999 (H9N2), produced recombinantly using the baculovirus expression system described previously (Ellebedy et al., 2014).

HA inhibition—We added serially diluted mAbs at an initial concentration of 30 μg/mL in PBS to V-shaped 96-well plates in duplicate. Next, we added 8 HA units/50 μL of 6:2 re-

assortant, low pathogenic (no multi-basic cleavage site) H5N1 virus (A/Indonesia/05/2005 and PR8 IBCDC-RG (H5N1)) to each well and incubated plates at room temperature for 30 min with shaking. We added 0.5% chicken red blood cells to each well and incubated plates at 4°C until red blood cells formed puncta at the bottom of the negative control wells. We measured minimum HAI concentration by determining the last dilution well that did not display hemagglutination.

mAb production—Antibodies were cloned as previously described (Wrammert et al., 2008). Total or H5 HA probe-binding plasmablasts were single cell sorted into 96-well plates containing RNA stabilizing buffer. VH, Vκ, and Vλ genes were then amplified by reverse transcription-PCR and nested PCR reactions from singly-sorted GC B cells and PBs using cocktails of primers specific for IgG, IgM/A, Igκ, and Igλ from previously detailed primer sets and then sequenced. The amplified VH, Vκ, and Vλ genes were cloned into IgG1 and Igκ expression vectors, respectively, as previously described. Heavy and light chain plasmids were co-transfected into Expi293F cells (GIBCO) for expression and antibody was purified with protein A agarose (Invitrogen).

Antibody affinity measurements—To measure binding affinities and off-rates of HA to Fabs, we first digested mAbs to Fab with immobilized papain (Thermo Fisher) and purified the digestion products over a protein A/G affinity column to isolate Fab. We biotinylated HA *in vitro* (EZ-Link-NHS-PEG4-Biotin, Thermo Fisher) and removed excess biotin with a desalting column (0.5mL Zeba Spin 7K MWCO, Thermo Fisher). We measured binding parameters of each Fab to HA by bio-layer interferometry (BLI) using an Octet Red96 instrument (ForteBio) or surface plasmon resonance (SPR) using a Biacore T200 SPR instrument (GE Healthcare). Using BLI, we performed a preliminary experiment to identify Fabs with too low signal-to-noise ratio to quantify; for higher sensitivity, we conducted SPR analyses for these Fabs. For BLI, we loaded 5 μg/mL biotinylated HA in HBS-EP buffer (10 mM HEPES pH 7.4, 150 mM NaCl, 3 mM EDTA, and 0.005% P20 surfactant) with 1% BSA onto streptavidin biosensors (ForteBio) for 1min. For SPR, we coupled neutravidin protein to CM5 sensor chips using standard amine-coupling and then captured biotinylated HA in HBS-EP buffer, which resulted in a response of 200–300 RU. We measured Fabs in 3-fold serial dilutions at 25°C and processed data using Biaevaluation 3.1 (GE Healthcare). We employed a 1:1 binding model to measure association and dissociation rate constants and fit steady-state equilibrium concentration curves.

Serum IgG purification, digestion, and complexing—To purify IgG from serum samples we heat inactivated 1 mL serum samples in a 55°C water bath for 30 min and incubated them on protein G resin (GE Healthcare) or Capture Select (Thermo Fisher) in a 1:1 ratio of serum to resin for 20 hours to bind IgG. After incubation, we removed IgG-depleted serum and washed IgG-bound protein G samples three times with PBS using centrifugation and Amicon concentrators. Next, to elute IgG from protein G resin, we incubated the samples in 0.1M glycine pH 2.5 buffer for 20 min followed by neutralization with 1M Tris-HCl pH 8 buffer, repeated twice. We buffer exchanged the samples into PBS using centrifugation with Amicon concentrators. For IgG digestion, we incubated 4 mg IgG with immobilized papain (Thermo Fisher) in freshly-prepared digestion buffer (20mM

sodium phosphate, 10 mM EDTA, 20 mM cysteine, pH 7.4) at 37°C for 18–22 hours. We separated digested IgG and immobilized papain using Pierce spin columns (Thermo Fisher) and buffer exchanged digested IgG into tris-buffered saline (TBS) using centrifugation with Amicon concentrators. To separate Fab/Fc from IgG we ran the samples through size exclusion chromatography with a Superdex 200 increase 10/300 column (GE Healthcare). For complexing, we concentrated 1mg Fab/Fc to ~50 μL and incubated with 20 μg recombinant HA at room temperature for 16–20 hours. Finally, we purified immune complexes from unbound Fab/Fc through size exclusion chromatography with a Superose 6 increase 10/300 column (GE Healthcare) and concentrated the immune complexes to ~50 μL.

mAb digestion and complexing for EM—To digest monoclonal IgG to Fab, we first incubated papain in freshly-prepared digestion buffer (100mM Tris pH 8, 2mM EDTA, 10mM L-cysteine) at 37°C for 15min. Next, we incubated activated papain with 1mg IgG in freshly-prepared digestion buffer at 37°C for 2 hours. To end the digestion, we added 50mM iodoacetamide. We buffer exchanged the digestion products into PBS using centrifugation with Amicon concentrators and purified Fabs using a CaptureSelect CH1-XL column (Thermo Fisher), eluting Fab with 150 mM sodium chloride and 20mM sodium acetate pH 3.4 buffer and neutralizing with 1M Tris-HCl pH 8 buffer. We buffer exchanged and concentrated Fab into PBS using centrifugation with Amicon concentrators and complexed Fab with HA at greater than 3× molar ratio of Fab to HA at 4°C for 16–20 hours.

Negative stain electron microscopy—To prepare grids for negative stain electron microscopy, we deposited purified immune complexes at ~30 μg/mL onto glow-discharged, carbon-coated 400 mesh copper grids (Electron Microscopy Sciences, EMS). After blotting to remove excess sample, we stained the grids with 2% w/v uranyl formate for 30 s followed by blotting to remove excess stain. We imaged the grids on a Talos 200C with a Falcon II direct electron detector and a CETA 4k camera (FEI) at 200kV, 73,000x magnification, and 1.98Å/pixel, a Tecnai Spirit T12 (FEI) with a CMOS 4k camera (TVIPS) at 120kV, 52,000× magnification, and 2.06Å/pixel, and a Tecnai T20 (FEI) with an Eagle CCD 4k camera (FEI) at 200kV, 62,000x magnification, and 1.77Å/pixel. We collected micrographs using Leginon, picked and stacked 100,000–400,000 single particles using Appion, and processed particles to reference-free 2D class averages and 3D reconstructions using Relion (Suloway et al., 2005; Lander et al., 2009; Scheres, 2012; Zivanov et al., 2018). We used UCSF Chimera to analyze data and generate figures (Pettersen et al., 2004). Due to low angular sampling induced by particle orientation bias and low abundance of immune complexes, a small proportion of immune complexes only partially reconstructed in 3D but clearly showed Fab placement relative to HA. These placements were also confirmed by distinct 2D class averages. Similarly to Gilchuk et al. (2019), we used our internal database of HA immune complexes, partial 3D density, and distinguishing 2D class averages as references to project these specificities onto 3D models of HA and mark them as predicted placements.

CryoEM—To freeze grids for cryoEM, we added Lauryl Maltose Neopentyl Glycol (Anatrace) at a final concentration of 5 μM to purified immune complexes at 750 μg/mL and deposited samples immediately onto glow-discharged 1.2/1.3 quantifoil 400 grids (EMS).

After incubating samples on grids for 7 s, we blotted off excess sample and froze grids in liquid ethane using a Vitrobot (FEI). We transferred grids to liquid nitrogen for storage. We imaged cryoEM grids on a Titan Krios (FEI) with a Gatan K2 summit detector operating at 300kV. We collected 2,559 micrographs in counting mode at 29,000 nominal magnification, 1.03Å/pixel, using Leginon (Suloway et al., 2005). Our total exposure time was 10.5 s with a total dose of 53.1 electrons/$Å^2$. After performing motion-correction and GCTF estimation, we picked particles using a difference-of-Gaussians picker (Voss et al., 2009; Zhang, 2016; Zheng et al., 2017). We performed initial reference-free 2D classification in Cryosparc followed by further 2D classification in Relion (Punjani et al., 2017; Zivanov et al., 2018). Next, we ran global 3D refinement with 3-fold symmetry expansion on the total particles after 2D cleanup. As pAb:HA complexes represented a minority of the total particles—mostly unbound HA and Fab—and were difficult to identify in 2D class averages, we turned to focus classification to guide identification, isolation, and refinement of each immune complex. In Relion, using the corresponding negative stain epitope landscape for subject 4 at day 28 as a guide, we positioned 40A sphere masks over expected pAbs and ran 3D classification without image alignment or imposed symmetry for each specificity. After identifying and classifying each unique pAb complex, we refined and post-processed each specificity with a mask around the entire immune complex. For our 4.7 Å resolution map of the stem-specific immune complex, we generated a predicted model of mAb 1C01 from subject 4 at day 7 using ROSIE (The Rosetta Online Server that Includes Everyone) and used Coot to minimally adjust the flexible CDR H3 loop into density (Emsley and Cowtan, 2004; Lyskov et al., 2013; Weitzner et al., 2017). As our resolution was not high enough, we did not further refine a model of 1C01 into the stem immune complex map.

QUANTIFICATION AND STATISTICAL ANALYSIS

We conducted statistical analyses in GraphPad Prism.

ADDITIONAL RESOURCES

More information about this clinical trial is located at clinicaltrials.gov under the identifier NCT01910519.

Supplementary Material

Refer to Web version on PubMed Central for supplementary material.

ACKNOWLEDGMENTS

Recombinant HA from A/Indonesia/5/2005 (H5N1) was provided by the International Reagent Resource. We thank Aleksandar Antanasijevic for invaluable assistance with focus classification data processing, Ian Wilson, Adrian McDermott, and James Crowe for providing recombinant HA protein, Bill Anderson for keeping the EM suite at Scripps Research running efficiently, and Alba Torrents de la Peña and Lauren Holden for critical reading of the manuscript. The Ward laboratory was funded by Collaborative Influenza Vaccine Innovation Centers contract 75N93019C00051. J.H. was funded by NIAID 2 T32 AI007244-36. The Ellebedy laboratory was supported by NIAID grants R21 AI139813 and U01 AI141990 and by NIAID Centers of Excellence for Influenza Research and Surveillance (CEIRS) contract HHSN272201400006C.

REFERENCES

Anderson CS, Ortega S, Chaves FA, Clark AM, Yang H, Topham DJ, and DeDiego ML (2017). Natural and directed antigenic drift of the H1 influenza virus hemagglutinin stalk domain. Sci. Rep. 7, 14614. [PubMed: 29097696]

Andrews SF, Huang Y, Kaur K, Popova LI, Ho IY, Pauli NT, Henry Dunand CJ, Taylor WM, Lim S, Huang M, et al. (2015). Immune history profoundly affects broadly protective B cell responses to influenza. Sci. Transl. Med. 7, 316ra192.

Belshe RB, Frey SE, Graham IL, Anderson EL, Jackson LA, Spearman P, Edupuganti S, Mulligan MJ, Rouphael N, Winokur P, et al.; National Institute of Allergy and Infectious Diseases–Funded Vaccine and Treatment Evaluation Units (2014). Immunogenicity of avian influenza A/Anhui/01/2005(H5N1) vaccine with MF59 adjuvant: a randomized clinical trial. JAMA 312, 1420–1428. [PubMed: 25291578]

Bianchi M, Turner HL, Nogal B, Cottrell CA, Oyen D, Pauthner M, Bastidas R, Nedellec R, McCoy LE, Wilson IA, et al. (2018). Electron-microscopy-based epitope mapping defines specificities of polyclonal antibodies elicited during HIV-1 BG505 envelope trimer immunization. Immunity 49, 288–300.e8. [PubMed: 30097292]

Boudreau CM, and Alter G (2019). Extra-neutralizing FcR-mediated antibody functions for a universal influenza vaccine. Front. Immunol. 10, 440. [PubMed: 30949165]

Bresson JL, Perronne C, Launay O, Gerdil C, Saville M, Wood J, Höschler K, and Zambon MC (2006). Safety and immunogenicity of an inactivated split-virion influenza A/Vietnam/1194/2004 (H5N1) vaccine: phase I randomised trial. Lancet 367, 1657–1664. [PubMed: 16714186]

Burton DR (2010). Scaffolding to build a rational vaccine design strategy. Proc. Natl. Acad. Sci. USA 107, 17859–17860. [PubMed: 20937874]

Centers for Disease Control and Prevention (2020). Past Seasons Vaccine Effectiveness Estimates, 2004–2019 (CDC). https://www.cdc.gov/flu/vaccines-work/past-seasons-estimates.html.

Cirelli KM, Carnathan DG, Nogal B, Martin JT, Rodriguez OL, Upadhyay AA, Enemuo CA, Gebru EH, Choe Y, Viviano F, et al. (2019). Slow delivery immunization enhances HIV neutralizing antibody and germinal center responses via modulation of immunodominance. Cell 177, 1153–1171.e28. [PubMed: 31080066]

Claas ECJ, Osterhaus AD, van Beek R, De Jong JC, Rimmelzwaan GF, Senne DA, Krauss S, Shortridge KF, and Webster RG (1998). Human influenza A H5N1 virus related to a highly pathogenic avian influenza virus. Lancet 351, 472–477. [PubMed: 9482438]

Coughlan L, and Palese P (2018). Overcoming barriers in the path to a universal influenza virus vaccine. Cell Host Microbe 24, 18–24. [PubMed: 30001520]

Cowling BJ, Jin L, Lau EH, Liao Q, Wu P, Jiang H, Tsang TK, Zheng J, Fang VJ, Chang Z, et al. (2013). Comparative epidemiology of human infections with avian influenza A H7N9 and H5N1 viruses in China: a population-based study of laboratory-confirmed cases. Lancet 382, 129–137. [PubMed: 23803488]

Cox F, Kwaks T, Brandenburg B, Koldijk MH, Klaren V, Smal B, Korse HJ, Geelen E, Tettero L, Zuijdgeest D, et al. (2016). HA antibody-mediated FcγRIIIa activity is both dependent on FcR engagement and interactions between HA and sialic acids. Front. Immunol. 7, 399. [PubMed: 27746785]

DiLillo DJ, Tan GS, Palese P, and Ravetch JV (2014). Broadly neutralizing hemagglutinin stalk-specific antibodies require FcγR interactions for protection against influenza virus in vivo. Nat. Med. 20, 143–151. [PubMed: 24412922]

Dreyfus C, Laursen NS, Kwaks T, Zuijdgeest D, Khayat R, Ekiert DC, Lee JH, Metlagel Z, Bujny MV, Jongeneelen M, et al. (2012). Highly conserved protective epitopes on influenza B viruses. Science 337, 1343–1348. [PubMed: 22878502]

Ekiert DC, Bhabha G, Elsliger MA, Friesen RH, Jongeneelen M, Throsby M, Goudsmit J, and Wilson IA (2009). Antibody recognition of a highly conserved influenza virus epitope. Science 324, 246–251. [PubMed: 19251591]

Ellebedy AH, Krammer F, Li GM, Miller MS, Chiu C, Wrammert J, Chang CY, Davis CW, McCausland M, Elbein R, et al. (2014). Induction of broadly cross-reactive antibody responses to

the influenza HA stem region following H5N1 vaccination in humans. Proc. Natl. Acad. Sci. USA 111, 13133–13138. [PubMed: 25157133]

Ellebedy AH, Nachbagauer R, Jackson KJL, Dai YN, Han J, Alsoussi WB, Davis CW, Stadlbauer D, Rouphael N, Chromikova V, et al. (2020). Adjuvanted H5N1 influenza vaccine enhances both cross-reactive memory B cell and strain-specific naive B cell responses in humans. Proc. Natl. Acad. Sci. USA 117, 17957–17964. [PubMed: 32661157]

Emsley P, and Cowtan K (2004). Coot: Model-building tools for molecular graphics. Acta Crystallogr. D Biol. Crystallogr. 60, 2126–2132. [PubMed: 15572765]

Erbelding EJ, Post DJ, Stemmy EJ, Roberts PC, Augustine AD, Ferguson S, Paules CI, Graham BS, and Fauci AS (2018). A universal influenza vaccine: The strategic plan for the national institute of allergy and infectious diseases. J. Infect. Dis. 218, 347–354. [PubMed: 29506129]

Gilchuk IM, Bangaru S, Gilchuk P, Irving RP, Kose N, Bombardi RG, Thornburg NJ, Creech CB, Edwards KM, Li S, et al. (2019). Influenza H7N9 virus neuraminidase-specific human monoclonal antibodies inhibit viral egress and protect from lethal influenza infection in mice. Cell Host Microbe 26, 715–728.e8. [PubMed: 31757769]

Gostic KM, Ambrose M, Worobey M, and Lloyd-Smith JO (2016). Potent protection against H5N1 and H7N9 influenza via childhood hemagglutinin imprinting. Science 354, 722–726. [PubMed: 27846599]

Gostic KM, Bridge R, Brady S, Viboud C, Worobey M, and Lloyd-Smith JO (2019). Childhood immune imprinting to influenza A shapes birth year-specific risk during seasonal H1N1 and H3N2 epidemics. PLoS Pathog. 15, e1008109. [PubMed: 31856206]

Huang KYA, Rijal P, Schimanski L, Powell TJ, Lin TY, McCauley JW, Daniels RS, and Townsend AR (2015). Focused antibody response to influenza linked to antigenic drift. J. Clin. Invest. 125, 2631–2645. [PubMed: 26011643]

Impagliazzo A, Milder F, Kuipers H, Wagner MV, Zhu X, Hoffman RM, van Meersbergen R, Huizingh J, Wanningen P, Verspuij J, et al. (2015). A stable trimeric influenza hemagglutinin stem as a broadly protective immunogen. Science 349, 1301–1306. [PubMed: 26303961]

Kanekiyo M, Joyce MG, Gillespie RA, Gallagher JR, Andrews SF, Yassine HM, Wheatley AK, Fisher BE, Ambrozak DR, Creanga A, et al. (2019). Mosaic nanoparticle display of diverse influenza virus hemagglutinins elicits broad B cell responses. Nat. Immunol. 20, 362–372. [PubMed: 30742080]

Krammer F (2019). The human antibody response to influenza A virus infection and vaccination. Nat. Rev. Immunol. 19, 383–397. [PubMed: 30837674]

Kurosaki T, Kometani K, and Ise W (2015). Memory B cells. Nat. Rev. Immunol. 15, 149–159. [PubMed: 25677494]

Lander GC, Stagg SM, Voss NR, Cheng A, Fellmann D, Pulokas J, Yoshioka C, Irving C, Mulder A, Lau PW, et al. (2009). Appion: an integrated, database-driven pipeline to facilitate EM image processing. J. Struct. Biol. 166, 95–102. [PubMed: 19263523]

Lee PS, and Wilson IA (2015). Structural characterization of viral epitopes recognized by broadly cross-reactive antibodies. Curr. Top. Microbiol. Immunol. 386, 323–341. [PubMed: 25037260]

Lee PS, Yoshida R, Ekiert DC, Sakai N, Suzuki Y, Takada A, and Wilson IA (2012). Heterosubtypic antibody recognition of the influenza virus hemagglutinin receptor binding site enhanced by avidity. Proc. Natl. Acad. Sci. USA 109, 17040–17045. [PubMed: 23027945]

Lee JM, Eguia R, Zost SJ, Choudhary S, Wilson PC, Bedford T, Stevens-Ayers T, Boeckh M, Hurt AC, Lakdawala SS, et al. (2019). Mapping person-to-person variation in viral mutations that escape polyclonal serum targeting influenza hemagglutinin. eLife 8, 1–28.

Li Y, Myers JL, Bostick DL, Sullivan CB, Madara J, Linderman SL, Liu Q, Carter DM, Wrammert J, Esposito S, et al. (2013). Immune history shapes specificity of pandemic H1N1 influenza antibody responses. J. Exp. Med. 210, 1493–1500. [PubMed: 23857983]

Lyskov S, Chou FC, Conchúir SÓ, Der BS, Drew K, Kuroda D, Xu J, Weitzner BD, Renfrew PD, Sripakdeevong P, et al. (2013). Serverification of molecular modeling applications: the Rosetta Online Server that Includes Everyone (ROSIE). PLoS ONE 8, e63906. [PubMed: 23717507]

Moyer TJ, Kato Y, Abraham W, Chang JYH, Kulp DW, Watson N, Turner HL, Menis S, Abbott RK, Bhiman JN, et al. (2020). Engineered immunogen binding to alum adjuvant enhances humoral immunity. Nat. Med. 26, 430–440. [PubMed: 32066977]

Nachbagauer R, and Palese P (2020). Is a universal influenza virus vaccine possible? Annu. Rev. Med 71, 315–327. [PubMed: 31600454]

Nachbagauer R, Wohlbold TJ, Hirsh A, Hai R, Sjursen H, Palese P, Cox RJ, and Krammer F (2014). Induction of broadly reactive anti-hemagglutinin stalk antibodies by an H5N1 vaccine in humans. J. Virol. 88, 13260–13268. [PubMed: 25210189]

Nogal B, Bianchi M, Cottrell CA, Kirchdoerfer RN, Sewall LM, Turner HL, Zhao F, Sok D, Burton DR, Hangartner L, and Ward AB (2020). Mapping polyclonal antibody responses in non-human primates vaccinated with HIV Env trimer subunit vaccines. Cell Rep. 30, 3755–3765.e7. [PubMed: 32187547]

Peiris JSM, de Jong MD, and Guan Y (2007). Avian influenza virus (H5N1): a threat to human health. Clin. Microbiol. Rev. 20, 243–267. [PubMed: 17428885]

Pettersen EF, Goddard TD, Huang CC, Couch GS, Greenblatt DM, Meng EC, and Ferrin TE (2004). UCSF Chimera—a visualization system for exploratory research and analysis. J. Comput. Chem. 25, 1605–1612. [PubMed: 15264254]

Punjani A, Rubinstein JL, Fleet DJ, and Brubaker MA (2017). cryoSPARC: algorithms for rapid unsupervised cryo-EM structure determination. Nat. Methods 14, 290–296. [PubMed: 28165473]

Scheres SHW (2012). RELION: implementation of a Bayesian approach to cryo-EM structure determination. J. Struct. Biol. 180, 519–530. [PubMed: 23000701]

Suloway C, Pulokas J, Fellmann D, Cheng A, Guerra F, Quispe J, Stagg S, Potter CS, and Carragher B (2005). Automated molecular microscopy: the new Leginon system. J. Struct. Biol. 151, 41–60. [PubMed: 15890530]

Sun J, Kudahl UJ, Simon C, Cao Z, Reinherz EL, and Brusic V (2014). Large-scale analysis of B-cell epitopes on influenza virus hemagglutinin - implications for cross-reactivity of neutralizing antibodies. Front. Immunol. 5, 38. [PubMed: 24570677]

Throsby M, van den Brink E, Jongeneelen M, Poon LL, Alard P, Cornelissen L, Bakker A, Cox F, van Deventer E, Guan Y, et al. (2008). Heterosubtypic neutralizing monoclonal antibodies cross-protective against H5N1 and H1N1 recovered from human IgM^+ memory B cells. PLoS ONE 3, e3942. [PubMed: 19079604]

Treanor JJ, Campbell JD, Zangwill KM, Rowe T, and Wolff M (2006). Safety and immunogenicity of an inactivated subvirion influenza A (H5N1) vaccine. N. Engl. J. Med. 354, 1343–1351. [PubMed: 16571878]

Voss NR, Yoshioka CK, Radermacher M, Potter CS, and Carragher B (2009). DoG Picker and TiltPicker: software tools to facilitate particle selection in single particle electron microscopy. J. Struct. Biol. 166, 205–213. [PubMed: 19374019]

Weitzner BD, Jeliazkov JR, Lyskov S, Marze N, Kuroda D, Frick R, Adolf-Bryfogle J, Biswas N, Dunbrack RL Jr., and Gray JJ (2017). Modeling and docking of antibody structures with Rosetta. Nat. Protoc. 12, 401–416. [PubMed: 28125104]

World Health Organization (2020). Cumulative number of confirmed human cases for avian influenza A (H5N1) reported to WHO, 2003–2020. https://www.who.int/influenza/human_animal_interface/EN_GIP_20160404cumulativenumberH5N1cases.pdf?ua=1.

Wilson PC, and Andrews SF (2012). Tools to therapeutically harness the human antibody response. Nat. Rev. Immunol. 12, 709–719. [PubMed: 23007571]

Wrammert J, Smith K, Miller J, Langley WA, Kokko K, Larsen C, Zheng NY, Mays I, Garman L, Helms C, et al. (2008). Rapid cloning of high-affinity human monoclonal antibodies against influenza virus. Nature 453, 667–671. [PubMed: 18449194]

Wu NC, Thompson AJ, Lee JM, Su W, Arlian BM, Xie J, Lerner RA, Yen HL, Bloom JD, and Wilson IA (2020). Different genetic barriers for resistance to HA stem antibodies in influenza H3 and H1 viruses. Science 368, 1335–1340. [PubMed: 32554590]

Yassine HM, Boyington JC, McTamney PM, Wei CJ, Kanekiyo M, Kong WP, Gallagher JR, Wang L, Zhang Y, Joyce MG, et al. (2015). Hemagglutinin-stem nanoparticles generate heterosubtypic influenza protection. Nat. Med. 21, 1065–1070. [PubMed: 26301691]

Yoshida R, Igarashi M, Ozaki H, Kishida N, Tomabechi D, Kida H, Ito K, and Takada A (2009). Cross-protective potential of a novel monoclonal antibody directed against antigenic site B of the hemagglutinin of influenza A viruses. PLoS Pathog. 5, e1000350. [PubMed: 19300497]

Zhang K (2016). Gctf: real-time CTF determination and correction. J. Struct. Biol. 193, 1–12. [PubMed: 26592709]

Zheng SQ, Palovcak E, Armache JP, Verba KA, Cheng Y, and Agard DA (2017). MotionCor2: anisotropic correction of beam-induced motion for improved cryo-electron microscopy. Nat. Methods 14, 331–332. [PubMed: 28250466]

Zhu X, Guo YH, Jiang T, Wang YD, Chan KH, Li XF, Yu W, McBride R, Paulson JC, Yuen KY, et al. (2013). A unique and conserved neutralization epitope in H5N1 influenza viruses identified by an antibody against the A/Goose/Guangdong/1/96 hemagglutinin. J. Virol. 87, 12619–12635. [PubMed: 24049169]

Zivanov J, Nakane T, Forsberg BO, Kimanius D, Hagen WJ, Lindahl E, and Scheres SH (2018). New tools for automated high-resolution cryo-EM structure determination in RELION-3. eLife 7, 1–22.

Zuo T, Sun J, Wang G, Jiang L, Zuo Y, Li D, Shi X, Liu X, Fan S, Ren H, et al. (2015). Comprehensive analysis of antibody recognition in convalescent humans from highly pathogenic avian influenza H5N1 infection. Nat. Commun. 6, 8855. [PubMed: 26635249]

Highlights

- Defined HA epitopes targeted by human polyclonal antibodies after H5N1 vaccination
- First H5N1 immunization elicited heterosubtypic polyclonal V_H1–69-like stem responses
- Second H5N1 immunization elicited polyclonal head responses mimicking H5N1 infection

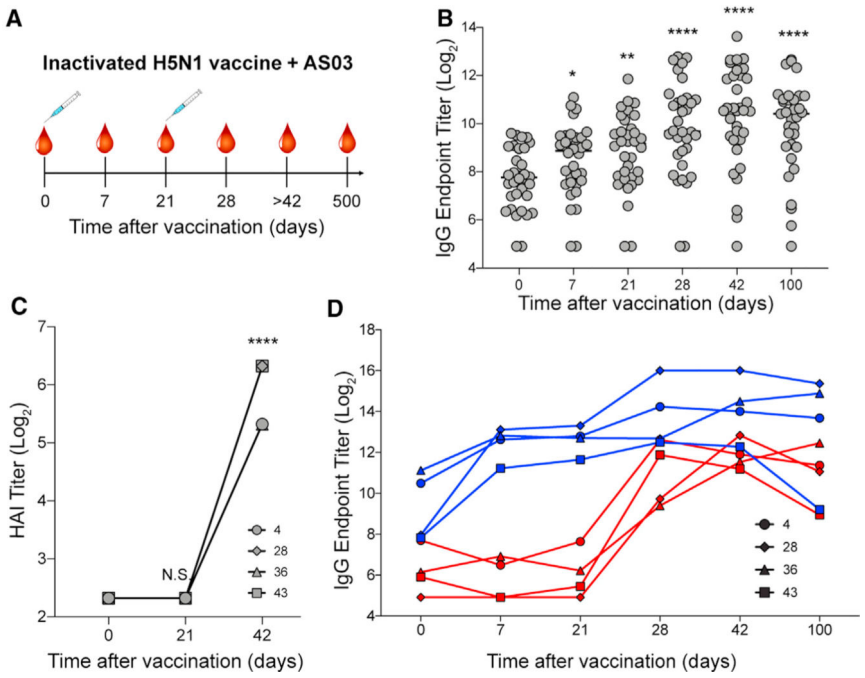

Figure 1. Novel H5N1 vaccination elicits robust IgG response to stem and head of hemagglutinin (HA)

(A) H5N1 vaccine trial: 34 healthy adults received the first immunization of inactivated H5N1 (A/Indonesia/5/2005) vaccine adjuvanted with AS03 at day 0 and the second immunization at day 21. Blood samples were collected on days 0, 7, 21, 28, 42 or 100, and 500 after vaccination.

(B) ELISA binding titers of serum IgG to recombinant H5 HA during the course of vaccination.

(C) HAI titers of serum IgG to recombinant H5 HA at days 0, 21, and 42 from subjects 4, 28, 36, and 43.

(D) ELISA binding titers of serum IgG to the head or stem domains of H5 HA using H5 head-specific (red) and stem-specific (blue) probes from subjects 4, 28, 36, and 43.

p values were determined by an unpaired t test: *$p < 0.05$, **$p < 0.01$, ****$p < 0.0001$. N.S., not significant. See also Figure S1.

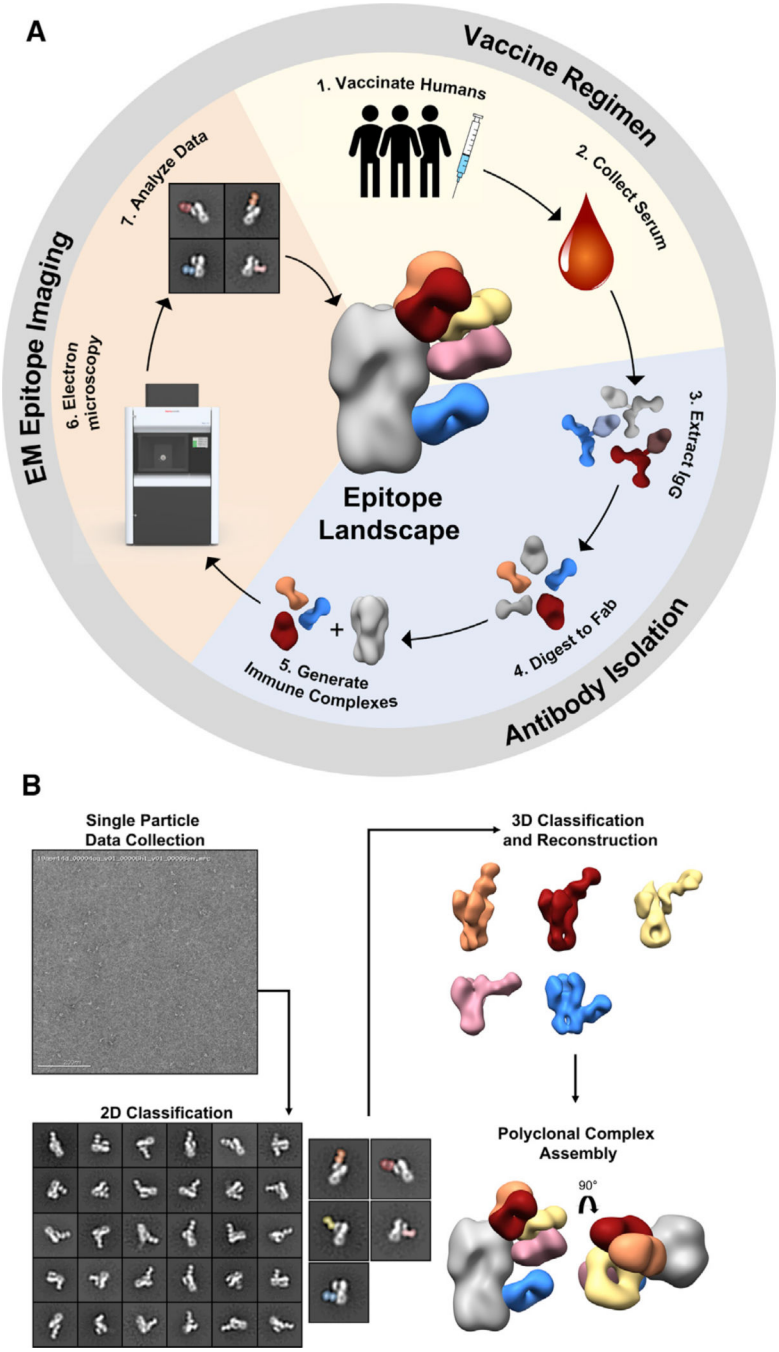

Figure 2. EM polyclonal epitope mapping (EMPEM) generates epitope landscapes from single particles

(A) Overview of EMPEM technique. In the vaccine regimen stage human subjects are immunized (1) and serum samples are collected throughout the course of the trial (2). During the antibody purification stage, IgG is extracted from serum samples (3) and digested with papain to Fab (4). Resulting Fabs are complexed with antigen (5). In the EM epitope imaging stage, immune complexes are imaged by EM (6), single-particle EM data are analyzed (7), and epitope landscapes are assembled.

(B) Overview of EM data processing steps. Single-particle EM data are collected, and particles are categorized into 2D class averages. Scale bar represents 200 nm. 2D classes of immune complexes are further categorized by another round of 2D classification and subjected to 3D classification and refinement. Finally, polyclonal complex assemblies are generated by segmenting and resampling densities corresponding to each Fab and mapped onto an HA trimer.

See also Figure S2.

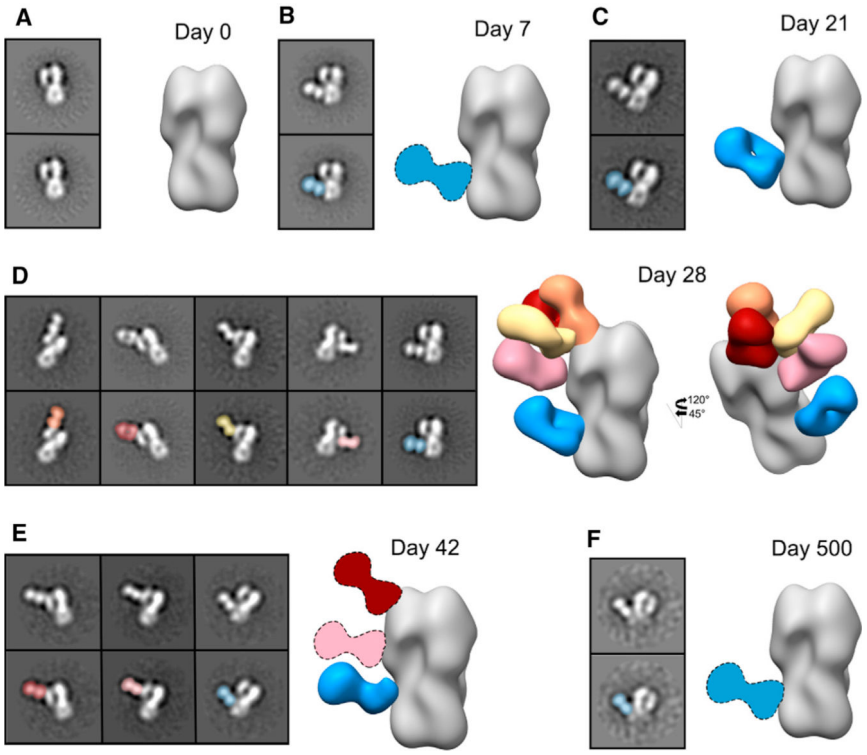

Figure 3. Kinetics of the polyclonal antibody (pAb) response to H5N1 vaccination in subject 4

Negative stain EM reconstructions of subject 4 pAbs in complex with recombinant H5 HA (A/Indonesia/5/2005) at days 0 (A), 7 (B), 21 (C), 28 (D), 42 (E), and 500 (F) after vaccination. Top left panel: representative 2D class average. Bottom left panel: 2D class average with the Fab labeled. Right panel: side view of polyclonal immune complexes. Stem specificity, blue; RBS-proximal and lateral patch specificities, red, orange, and yellow; vestigial esterase specificity, pink. Due to limited particle representation, Fab graphics with dashed outlines are predicted placements. See also Figure S3.

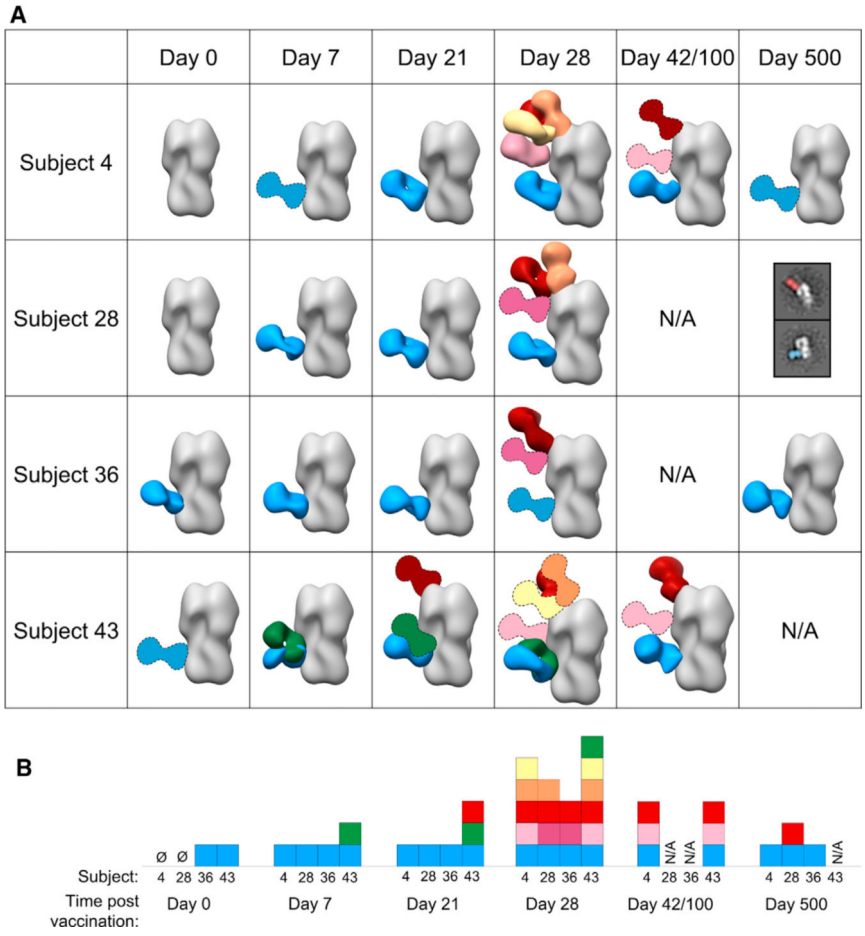

Figure 4. Polyclonal antibodies elicited by H5N1 vaccination decorate the stem, head, and vestigial esterase domains of HA

(A) Matrix of negative stain EM reconstructions of pAbs in complex with recombinant H5 HA (A/Indonesia/5/2005) from each subject at all time points listed. 3D reconstructions of polyclonal immune complexes are shown for most time points. Due to limited particle representation, Fab graphics with dashed outlines are predicted placements. For samples with immune complexes in low abundance, example 2D class averages with labels are shown.

(B) Summary of epitopes targeted by pAbs. Each square represents a Fab specificity from the corresponding subject and time point. Stem specificities, blue and green; RBS-proximal and lateral patch specificities, red, orange, and yellow; vestigial esterase and mid-lateral head specificities, light pink and dark pink.

See also Figure S4.

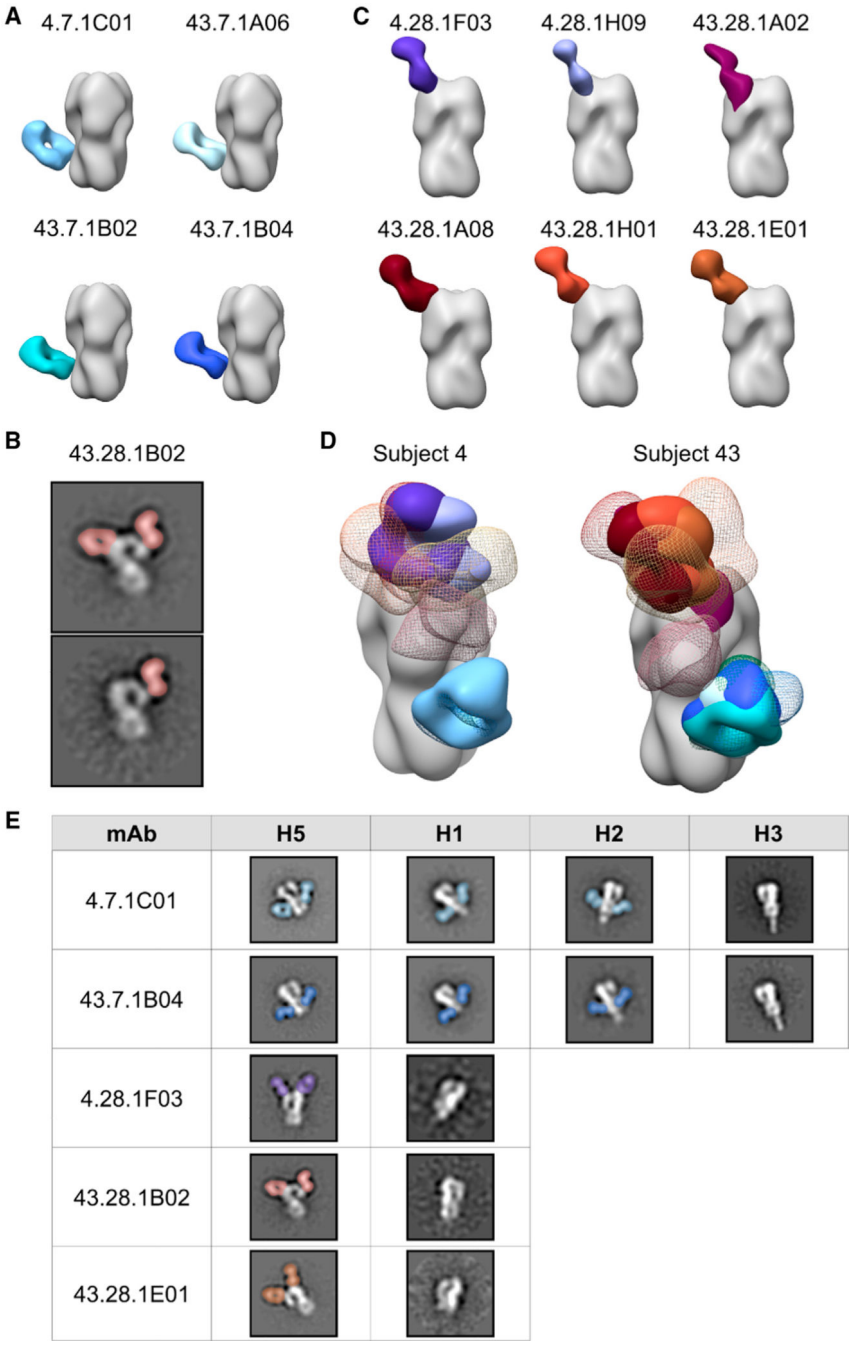

Figure 5. H5N1 vaccine-elicited mAbs target discrete regions on HA and share footprints with pAbs

(A–C) Side views of negative stain EM reconstructions or 2D class averages show that subjects 4 and 43 day 7 mAbs target the stem domain (A) while day 28 mAbs target the vestigial esterase domain (B) and the RBS (C) of recombinant H5 HA (A/Indonesia/5/2005). (D) Comparison of subjects 4 and 43 mAb and pAb immune complexes. Due to limited particle representation, orange, yellow, and pink pAbs from subject 43 are predicted placements.

(E) Cross-reactivity of example mAbs from subjects 4 and 43 to recombinant HAs from A/Indonesia/5/2005 (H5N1), A/California/04/2009 (H1N1), A/Singapore/1/1957 (H2N2), and A/Singapore/INFIMH-16–0019/2016 (H3N2). mAbs are shown in solid colors: 4.7.1C01, pale blue; 43.7.1A06, light blue; 43.7.1B02, teal; 43.7.1B04, dark blue; 4.28.1F03, purple; 4.28.1H09, lavender; 43.28.1A02, plum; 43.28.1A08, maroon; 43.28.1H01, brick; and 43.28.1E01, brown. pAbs from day 28 are shown in colored mesh: stem specificities, blue and green; RBS-proximal and lateral patch specificities, red, orange, and yellow; vestigial esterase and mid-lateral head specificities, pink.
See also Figure S5.

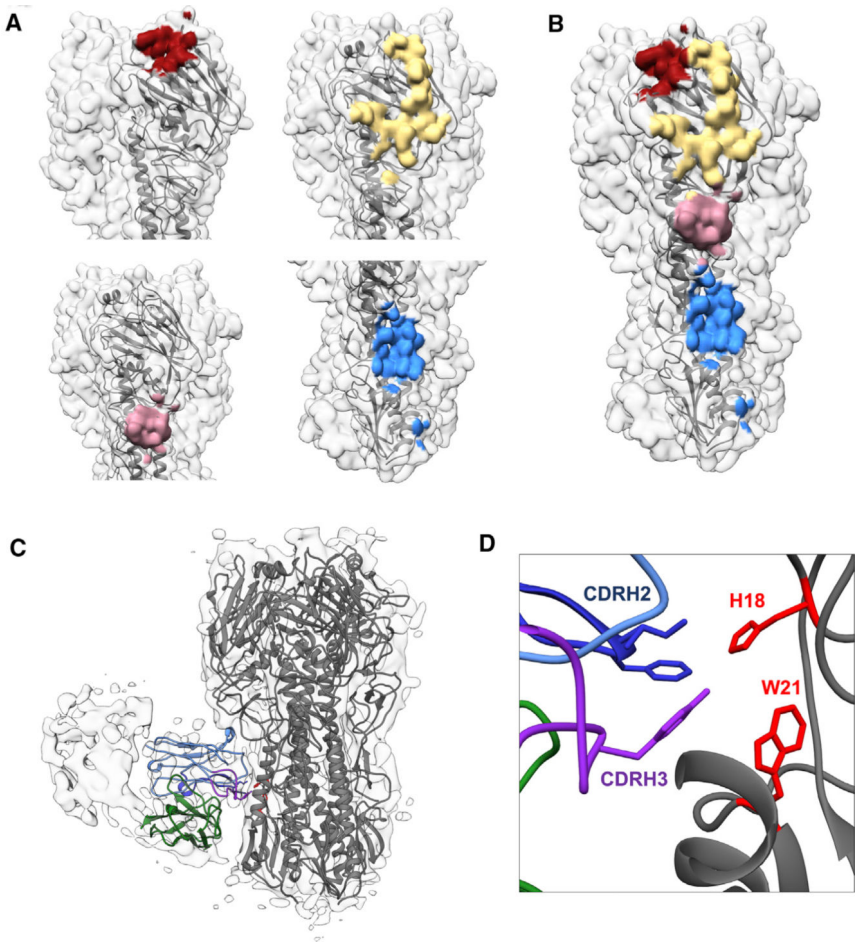

Figure 6. High-resolution cryoEM defines broadly reactive epitopes of H5N1 vaccine-elicited pAbs

(A) CryoEM-mapped epitopes targeted by pAbs from subject 4 at day 28. RBS epitope, red; lateral patch epitope, yellow; vestigial esterase epitope, pink; V_H1–69 epitope, blue.

(B) Each epitope specificity marked together on a single trimer.

(C and D) CryoEM map of stem immune complex from subject 4 at day 28 with ribbon diagrams for H5 HA (A/Indonesia/5/2005, gray; PDB: 4K62) and mAb 1C01 from subject 4 day 7 docked into the EM density. Full-length side view (C) and zoomed in view of the epitope-paratope interaction (D). V_H, blue; V_L, green; CDRH2, dark blue; CDRH3, purple; HA residues H18 and W21, red.

See also Figure S6.

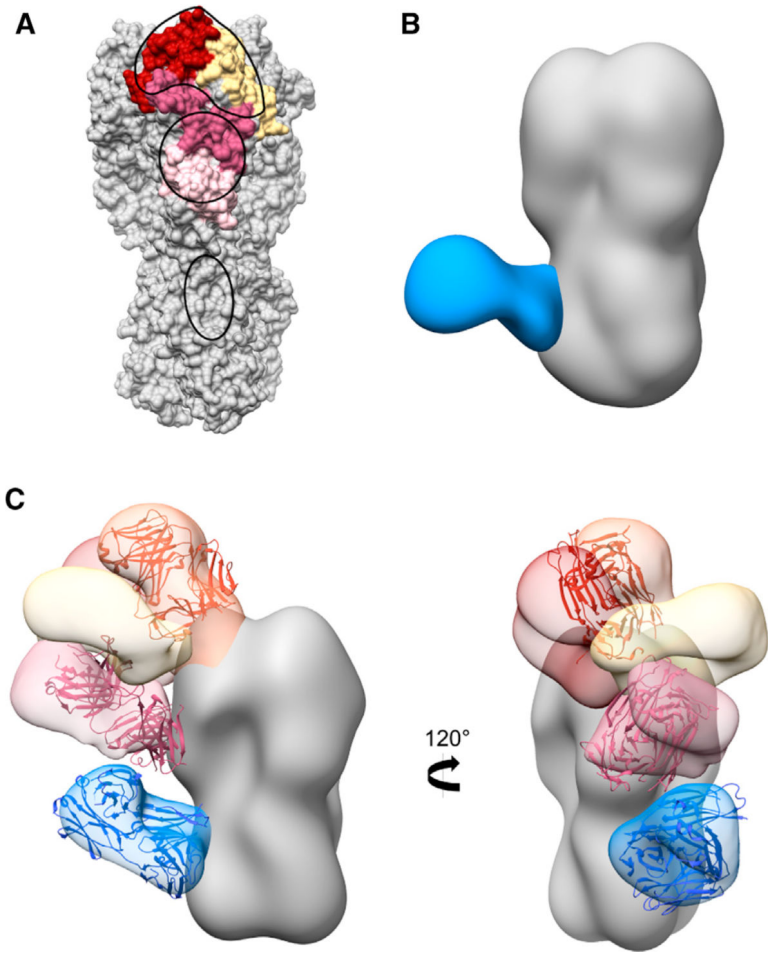

Figure 7. H5N1 vaccine-elicited pAb response mimics natural infection and generates heterosubtypic immunity

(A) H5 HA (A/Indonesia/5/2005) with vulnerable sites (VSs) marked in yellow for VS1, red for VS2, dark pink for VS3, and light pink for VS4. Footprints of pAbs from all subjects at day 28 are outlined in black.

(B) Negative stain EM reconstruction of subject 43 pAbs in complex with recombinant H1 HA (A/Michigan/45/2015) at day 21. Stem specificity, blue.

(C) Subject 4, day 28 negative stain epitope landscape with broadly neutralizing antibodies docked into HA density. bnAb S139/1 (PDB 4GMS), orange; bnAb H5M9 (4MHH), pink; bnAbCR9114 (4FQI), blue.

See also Figure S7.

KEY RESOURCES TABLE

REAGENT or RESOURCE	SOURCE	IDENTIFIER
Antibodies		
10.04.7.1C01 mAb	Ellebedy laboratory (Ellebedy et al., 2020)	N/A
10.04.28.1F03 mAb	Ellebedy laboratory (Ellebedy et al., 2020)	N/A
10.04.28.1H09 mAb	Ellebedy laboratory (Ellebedy et al., 2020)	N/A
10.43.7.1A06 mAb	Ellebedy laboratory (Ellebedy et al., 2020)	N/A
10.43.7.1B02 mAb	Ellebedy laboratory (Ellebedy et al., 2020)	N/A
10.43.7.1B04 mAb	Ellebedy laboratory (Ellebedy et al., 2020)	N/A
10.43.28.1B02 mAb	Ellebedy laboratory (Ellebedy et al., 2020)	N/A
10.43.28.1A08 mAb	Ellebedy laboratory (Ellebedy et al., 2020)	N/A
10.43.28.1A02 mAb	Ellebedy laboratory (Ellebedy et al., 2020)	N/A
10.43.28.1E01 mAb	Ellebedy laboratory (Ellebedy et al., 2020)	N/A
10.43.28.1H01 mAb	Ellebedy laboratory (Ellebedy et al., 2020)	N/A
Peroxidase AffiniPure Goat Anti-Human IgG (H+L)	Jackson ImmunoResearch	Cat #109-035-088
SIGMA*FAST* OPD	Sigma Aldrich	Cat #P9187
Bacterial and virus strains		
6:2 re-assortant, low pathogenic (no multi-basic cleavage site) H5N1 virus (A/Indonesia/05/2005 and PR8 IBCDC-RG (H5N1))	Rafi Ahmed laboratory (Ellebedy et al., 2020)	N/A
Biological samples		
Serum from human subjects	Rafi Ahmed laboratory (Ellebedy et al., 2020)	NCT01910519
Chemicals, peptides, and recombinant proteins		
H5N1 monovalent, inactivated vaccine	GlaxoSmithKline	N/A
AS03	GlaxoSmithKline	N/A
HA from A/Indonesia/5/2005 (H5N1)	International Reagent Resource	FR-59
Trimeric head domain of HA from A/Indonesia/5/2005	Rafi Ahmed laboratory (Ellebedy et al., 2014)	N/A
Chimeric HA: stem from A/Indonesia/5/2005, head from A/guinea fowl/Hong Kong/WF10/1999 (H9N2)	Rafi Ahmed laboratory (Ellebedy et al., 2014)	N/A
HA from A/California/04/2009 (H1N1)	Produced in house	N/A
HA from A/Michigan/45/2015 (H1N1)	Ian Wilson laboratory	N/A
HA from A/Singapore/1/1957 (H2N2)	Adrian McDermott laboratory	N/A
HA from A/Singapore/INFIMH-16-0019/2016 (H3N2)	James Crowe laboratory	N/A
Protein G Resin 4 FastFlow	GE Healthcare	Cat #17-0618-05
CaptureSelect IgG-Fc (ms) Affinity Matrix	Thermo Fisher	Cat #1912855250

REAGENT or RESOURCE	SOURCE	IDENTIFIER
Immobilized papain	Thermo Fisher	Cat #20341
Papain from papaya latex	Sigma Aldrich	Cat #P3125
Superose 6 increase 10/300 size exclusion column	GE Healthcare	Cat #17-5172-01
Superdex 200 increase 10/300 size exclusion column	GE Healthcare	Cat #17-5175-01
CaptureSelect CH1-XL column	Thermo Fisher	Cat #494346201
Uranyl Formate	Electron Microscopy Sciences	Cat #D310 25 GM
Lauryl Maltose Neopentyl Glycol	Anatrace	Cat #NG310 5 GM
Zeba Spin Desalting Columns, 7K MWCO	Thermo Fisher	Cat #89883
20X HBS-EP buffer	Teknova	Cat #H8022
Bovine Serum Albumins	Sigma Aldrich	Cat #A7906
Critical commercial assays		
EZ-Link-NHS-PEG4-Biotin	Thermo Fisher	Cat # 21363
Streptavidin (SA) Biosensors	ForteBio	Cat #18-5019
CM5 sensor chips	GE Healthcare	Cat #29149604
Deposited data		
Polyclonal immune complex of Fab binding the stem of H5 HA from serum of subject 4 at day 21	EMDataBank	EMD-22536
Polyclonal immune complex of Fab binding the stem of H5 HA from serum of subject 4 at day 28	EMDataBank	EMD-22537
Polyclonal immune complex of Fab binding the side of the head of H5 HA from serum of subject 4 at day 28	EMDataBank	EMD-22538
Polyclonal immune complex of Fab binding the side of the head of H5 HA from serum of subject 4 at day 28	EMDataBank	EMD-22539
Polyclonal immune complex of Fab binding the receptor binding site region of H5 HA from serum of subject 4 at day 28	EMDataBank	EMD-22540
Polyclonal immune complex of Fab binding the top of the head of H5 HA from serum of subject 4 at day 28	EMDataBank	EMD-22541
Polyclonal immune complex of Fab binding the stem of H5 HA from serum of subject 4 at day 42	EMDataBank	EMD-22542
Polyclonal immune complex of Fab binding the stem of H5 HA from serum of subject 28 at day 7	EMDataBank	EMD-22543
Polyclonal immune complex of Fab binding the stem of H5 HA from serum of subject 28 at day 21	EMDataBank	EMD-22544
Polyclonal immune complex of Fab binding the stem of H5 HA from serum of subject 28 at day 28	EMDataBank	EMD-22545
Polyclonal immune complex of Fab binding the receptor binding site region of H5 HA from serum of subject 28 at day 28	EMDataBank	EMD-22546
Polyclonal immune complex of Fab binding the top of the head of H5 HA from serum of subject 28 at day 28	EMDataBank	EMD-22547
Polyclonal immune complex of Fab binding the stem of H5 HA from serum of subject 36 at day 0	EMDataBank	EMD-22548
Polyclonal immune complex of Fab binding the stem of H5 HA from serum of subject 36 at day 7	EMDataBank	EMD-22549
Polyclonal immune complex of Fab binding the stem of H5 HA from serum of subject 36 at day 21	EMDataBank	EMD-22550
Polyclonal immune complex of Fab binding the receptor binding site region of H5 HA from serum of subject 36 at day 28	EMDataBank	EMD-22551

REAGENT or RESOURCE	SOURCE	IDENTIFIER
Polyclonal immune complex of Fab binding the stem of H5 HA from serum of subject 36 at day 500	EMDataBank	EMD-22552
Polyclonal immune complex of Fab binding the stem of H5 HA from serum of subject 43 at day 7	EMDataBank	EMD-22553
Polyclonal immune complex of Fab binding the stem of H5 HA from serum of subject 43 at day 7	EMDataBank	EMD-22554
Polyclonal immune complex of Fab binding the stem of H5 HA from serum of subject 43 at day 21	EMDataBank	EMD-22555
Polyclonal immune complex of Fab binding the stem of H5 HA from serum of subject 43 at day 28	EMDataBank	EMD-22556
Polyclonal immune complex of Fab binding the stem of H5 HA from serum of subject 43 at day 28	EMDataBank	EMD-22557
Polyclonal immune complex of Fab binding the receptor binding site region of H5 HA from serum of subject 43 at day 28	EMDataBank	EMD-22558
Polyclonal immune complex of Fab binding the stem of H5 HA from serum of subject 43 at day 100	EMDataBank	EMD-22559
Polyclonal immune complex of Fab binding the receptor binding site region of H5 HA from serum of subject 43 at day 100	EMDataBank	EMD-22560
Monoclonal immune complex of Fab 1A06 from participant 43 at day 7 binding the stem of H5 HA	EMDataBank	EMD-22561
Monoclonal immune complex of Fab 1B02 from participant 43 at day 7 binding the stem of H5 HA	EMDataBank	EMD-22562
Monoclonal immune complex of Fab 1B04 from participant 43 at day 7 binding the stem of H5 HA	EMDataBank	EMD-22563
Monoclonal immune complex of Fab 1A02 from participant 43 at day 28 binding the stem of H5 HA	EMDataBank	EMD-22564
Monoclonal immune complex of Fab 1A08 from participant 43 at day 28 binding the stem of H5 HA	EMDataBank	EMD-22565
Monoclonal immune complex of Fab 1H01 from participant 43 at day 28 binding the stem of H5 HA	EMDataBank	EMD-22566
Monoclonal immune complex of Fab 1E01 from participant 43 at day 28 binding the stem of H5 HA	EMDataBank	EMD-22567
Polyclonal immune complex of Fab binding the stem of H1 HA from serum of subject 43 at day 21	EMDataBank	EMD-22568
CryoEM polyclonal immune complex of Fab binding the stem of H5 HA from serum of subject 4 at day 28	EMDataBank	EMD-22569
CryoEM polyclonal immune complex of Fab binding the stem of H5 HA from serum of subject 4 at day 28	EMDataBank	EMD-22570
CryoEM polyclonal immune complex of Fab binding the stem of H5 HA from serum of subject 4 at day 28	EMDataBank	EMD-22571
CryoEM polyclonal immune complex of Fab binding the stem of H5 HA from serum of subject 4 at day 28	EMDataBank	EMD-22572
Experimental models: cell lines		
Chicken red blood cells	Lampire	Cat #7241408
Freestyle 293-F cells	Thermo Fisher	Cat# R79007
Software and algorithms		
Unicorn 7.0	GE Healthcare	https://www.cytivalifesciences.com/
Leginon	Suloway et al. (2005)	N/A
Appion	Lander et al. (2009)	N/A
DoG Picker	Voss et al. (2009)	N/A
Relion	Scheres (2012)	N/A

REAGENT or RESOURCE	SOURCE	IDENTIFIER
Cryosparc2	Punjani et al. (2017)	N/A
UCSF Chimera	Pettersen et al. (2004)	N/A
Other		
Negative stain EM grids, 400 mesh	Electron Microscopy Sciences	Cat #EMS400-CU
CryoEM grids, quantifoil 1.2/1.3, 00 mesh	Electron Microscopy Sciences	Q4100CR1.3-2nm